

**Pressure-induced permanent annihilation of free volume in La<sub>75</sub>Al<sub>25</sub> metallic glasses**Fujun Lan,<sup>1</sup> Hongbo Lou <sup>1</sup> Dazhe Xu,<sup>1</sup> Tao Liang <sup>1</sup> Fei Zhang,<sup>2</sup> Ziliang Yin,<sup>1</sup> Ye Liu,<sup>1</sup> Xin Zhang,<sup>1</sup> Yanping Yang,<sup>1</sup> Sheng Jiang,<sup>3</sup> Ke Yang,<sup>3</sup> Jianrong Zeng,<sup>3</sup> Aiguo Li,<sup>3</sup> Zhidan Zeng,<sup>1</sup> and Qiaoshi Zeng <sup>1,4,\*</sup><sup>1</sup>*Center for High Pressure Science and Technology Advanced Research, Pudong, Shanghai 201203, China*<sup>2</sup>*Multi-discipline Research Center, Institute of High Energy Physics, Chinese Academy of Sciences, Beijing 100049, China*<sup>3</sup>*Shanghai Synchrotron Radiation Facility, Shanghai Advanced Research Institute, Chinese Academy of Sciences, Shanghai 201204, China*<sup>4</sup>*Shanghai Key Laboratory of Material Frontiers Research in Extreme Environments (MFree), Institute for Shanghai Advanced Research in Physical Sciences (SHARPS), Shanghai 201203, China*

(Received 9 January 2024; revised 6 May 2024; accepted 15 May 2024; published 3 June 2024)

Free volume is one of the most important structural features closely associated with various glass phenomena and properties. However, precise determination of how free volume evolves with external tuning poses a considerable challenge. In this work, by using *in situ* high-pressure synchrotron x-ray diffraction in a diamond anvil cell, we investigate the effect of pressure on free volume in a relatively soft La<sub>75</sub>Al<sub>25</sub> metallic glass (MG). Our investigation quantitatively compares the pressure-dependent principal diffraction peak position and peak width variations with high accuracy between as-quenched and thermally annealed La<sub>75</sub>Al<sub>25</sub> metallic glass samples (each possessing different initial free-volume contents but under identical hydrostatic pressure conditions). The differences in compression and decompression behaviors are elucidated and discussed within the framework of free volume. It is revealed that free volume engages in the compression process with a linear, pressure-dependent reduction below ~10 GPa, after which it reaches a saturated flat stage, maintaining a constant content up to 23.1 GPa. During decompression, an obvious hysteresis loop and permanent densification are observed. Although under hydrostatic pressure conditions, both La<sub>75</sub>Al<sub>25</sub> metallic glasses exhibit an inevitable buildup of local stress and/or strain once pressure is applied, and the annealed sample displays a notably faster rate of increase. Evident residual local stress and/or strain persists in the annealed sample after pressure release. Our findings underscore the complicated compression and decompression behavior in MGs if the pressure is high enough with respect to the sample bulk modulus. These complexities unveil many details regarding glass structures, especially the content and distribution of free volume, providing valuable insights to deepen our comprehension of free volume in glass structures.

DOI: [10.1103/PhysRevB.109.214201](https://doi.org/10.1103/PhysRevB.109.214201)**I. INTRODUCTION**

In principle, every substance can form a glass if its melt can be rapidly quenched to bypass the regular rearrangement of atoms and/or molecules required for crystallization. In a simplified picture, a glass can be regarded as a rigid “frozen” state of melt with viscosity increased by many orders of magnitude over a narrow temperature range (glass transition range) during melt quenching. The sharp increase of viscosity, i.e., the glass formation, is believed to be closely associated with the decrease of free volume below some critical value when approaching the glass transition temperature [1]. The free-volume concept was first proposed by Eyring in the 1930s to understand the properties of liquids as “the liquid molecule is thought to move in a box of length  $d$  where we can think of  $d^3$  as the free space per molecule” [2]. Since then, the concept of free volume has been extensively developed and sometimes defined differently in the literature [3,4]. Nevertheless, it always associates with the variable empty space

between atoms and/or molecules and has provided a simple theoretical framework to describe various liquid and glass behavior and properties, such as diffusion [5,6], viscosity [7], glass transition [8–11], relaxation [12–14], rejuvenation [15], deformation [16–19], and glass structure [20,21]. However, due to the complexity of the disordered glass structure, free volume is structurally ill defined [22] and also challenging to be directly and accurately determined by experiments [7,13,23–25], which remains a long-standing challenge in the glass community [26].

Among various glasses, metallic glasses (MGs), characterized by random close-packing atomic structures with nondirectional metallic bonds, have been regarded as the simplest atomic glass systems, making them an ideal model for fundamental studies of glass-related problems [8]. Regardless of the packing details, the total volume of an MG can be simply divided into two distinct components: the atomic occupied volume ( $V_0$ ) and the quenched-in free volume ( $V_f$ ).  $V_0$  comprises the volume occupied by the atomic cores and their thermal vibrations.  $V_0$  is basically structure independent and primarily influenced by thermal expansion and is typically considered to behave elastically under stress. In contrast,  $V_f$  is highly structure and/or state sensitive, which could be

\*Corresponding author: zengqs@hpstar.ac.cn

annihilated or reduced through thermal annealing below the glass transition temperature ( $T_g$ ) by structural rearrangement [27] and restored through heating above  $T_g$  or cryogenic thermal cycling via atomic diffusion or nonaffine displacement [28]. However, how  $V_f$  is spatially distributed in glass is still an open question.

It was believed that the rigid backbone or matrix of glass mainly consists of  $V_0$ , while  $V_f$  only exists as low-content defects [5]. Therefore, glasses with identical composition but different thermal histories (differences in the contents of  $V_f$ ) usually show identical thermal expansion coefficients [13], and their compression behavior is also expected to be similar (independent of thermal history) as controlled by the rigid backbone [29]. However, MGs with different thermal histories (as-quenched and annealed states) have been found to show quite different bulk moduli [30,31]. Moreover, permanent densification was claimed in MGs by the Archimedes density measurement method after high-pressure treatment, even at room temperature, which was attributed to the pressure-induced annihilation or reduction of free volume [32,33]. These results suggest that  $V_f$  also engages in the compression process besides the rigid  $V_0$  and, therefore, is in line with the popular heterogeneous structural model of MGs. That is,  $V_f$  is not homogeneously distributed; instead,  $V_f$  could aggregate in loosely packed liquidlike soft ( $V_0$  plus relatively more  $V_f$ ) regions (their volume fraction could be as high as  $\sim 25\%$ ), embedded in the densely packed solidlike hard ( $V_0$  plus relatively less  $V_f$ ) regions (a natural consequence of the glass transition during melt quenching based on the percolation model [8]). Both regions respond to external stimuli and determine the properties of MGs [18,19]. However, our recent *in situ* high-pressure synchrotron x-ray diffraction (XRD) measurements on a Zr-based MG did not observe any permanent densification; instead, a reversible linear compression behavior of  $V_f$  was present and challenges our expectation based on the prevailing structure models of MGs [31]. Clarifying whether the reversible linear compression behavior is general for MGs (valid for various MGs at broader pressure range) is crucial to establish a more realistic structural model for MGs, which, however, is still unclear. Further investigation on the behavior of  $V_f$  of MGs under external stimuli can not only help validate and develop the free-volume theory but also uncover detailed information on the glass structure and its relationship with glass properties [31].

Among the techniques employed to characterize  $V_f$  in MGs [13,23,24,27,34], synchrotron XRD is one of the most accurate and direct probes to monitor the relative change of  $V_f$  in MGs at the atomic scale compatible with various sample environments [13,24]. Specifically, the principal XRD peak position of MGs,  $q_1$ , in the  $q$  space (reciprocal space) can be accurately determined with the resolution better than  $10^{-4}$  Å by using synchrotron XRD. Then, the relative change in specific sample volume (density) or averaged atomic spacing tuned by temperature [13], stress [35], and pressure [36,37] can be readily calculated by their simple relationships with  $q_1$ . Pressure is a clean thermodynamic parameter capable of effectively modulating the density and structure of MGs [38–42], therefore providing an ideal tuning tool for  $V_f$  in MGs [31]. Reaching extremely high pressures and simultaneously maintaining good pressure hydrostaticity are challenging.

Therefore, in this work, instead of going to higher pressures to validate the generality of the linear compression behavior of  $V_f$ , we choose a much softer and simple binary MG sample,  $\text{La}_{75}\text{Al}_{25}$ , as a model system and employ an *in situ* high-pressure synchrotron XRD technique with a diamond anvil cell (DAC) to investigate the structural changes with different free-volume contents (as-quenched and annealed states). The compression and decompression behaviors between the two samples are carefully compared, and the underlying mechanism is discussed based on the framework of free volume.

## II. EXPERIMENTAL METHODS

### A. Sample preparation

Master ingots with a nominal atomic composition of  $\text{La}_{75}\text{Al}_{25}$  were prepared by arc-melting high-purity ( $>99.9$  at. %) elements in a Ti-gettered high-purity Ar atmosphere. Each ingot was flipped and remelted six times to ensure chemical homogeneity. As-quenched MG ribbons with a thickness of  $\sim 30$   $\mu\text{m}$  were produced using the single-roller melt-spinning method at a wheel speed of  $\sim 50$  m/s. The sample with a relatively lower free-volume content was obtained by thermal annealing treatment of the as-quenched ribbons. Specifically, the as-quenched ribbons were heated from room temperature (20 K/min) to 453 K ( $\sim 21$  K below  $T_g$ ,  $\sim 474$  K) and maintained there for 5 min, then cooled down to room temperature under a flowing high-purity Ar atmosphere in a differential scanning calorimetry (DSC) instrument (Perkin-Elmer 8500).

### B. Sample characterization

The amorphous structure of the as-quenched and annealed ribbon samples was confirmed by synchrotron XRD and transmission electron microscopy (TEM). For TEM measurements, the two samples were prepared using a focused ion beam (FEI, Versa 3D). High-resolution transmission electron microscopy (HRTEM) images and selected area electron diffraction (SAED) images were obtained using a Tecnai F20 (FEI) TEM. Synchrotron XRD measurements at ambient conditions were performed at beamline 15U1 at the Shanghai Synchrotron Radiation Facility (SSRF), China. The monochromatic x-ray wavelength was 0.6199 Å, and the exposure time for each sample was 30 s. The structural homogeneity at the nanoscale of the two samples was confirmed by synchrotron small-angle x-ray scattering (SAXS) experiments conducted at beamline 12ID-B at the Advanced Photon Source (APS), Argonne National Laboratory (ANL), USA, with an x-ray wavelength of 1.0332 Å and exposure time of 60 s for each pattern. Thermal properties of the samples were characterized using the DSC instrument, with a typical heating rate of 20 K/min. Mechanical properties were examined by nanoindentation experiments conducted on an instrumented nanoindenter (G200, Keysight, USA) equipped with a standard Berkovich diamond indenter. The sample surfaces for nanoindentation tests were meticulously polished to achieve a mirror finish. The displacement-control mode was utilized with a maximum load of 15 mN at a strain rate of 0.2  $\text{s}^{-1}$ . The hardness of the samples was determined by analyzing

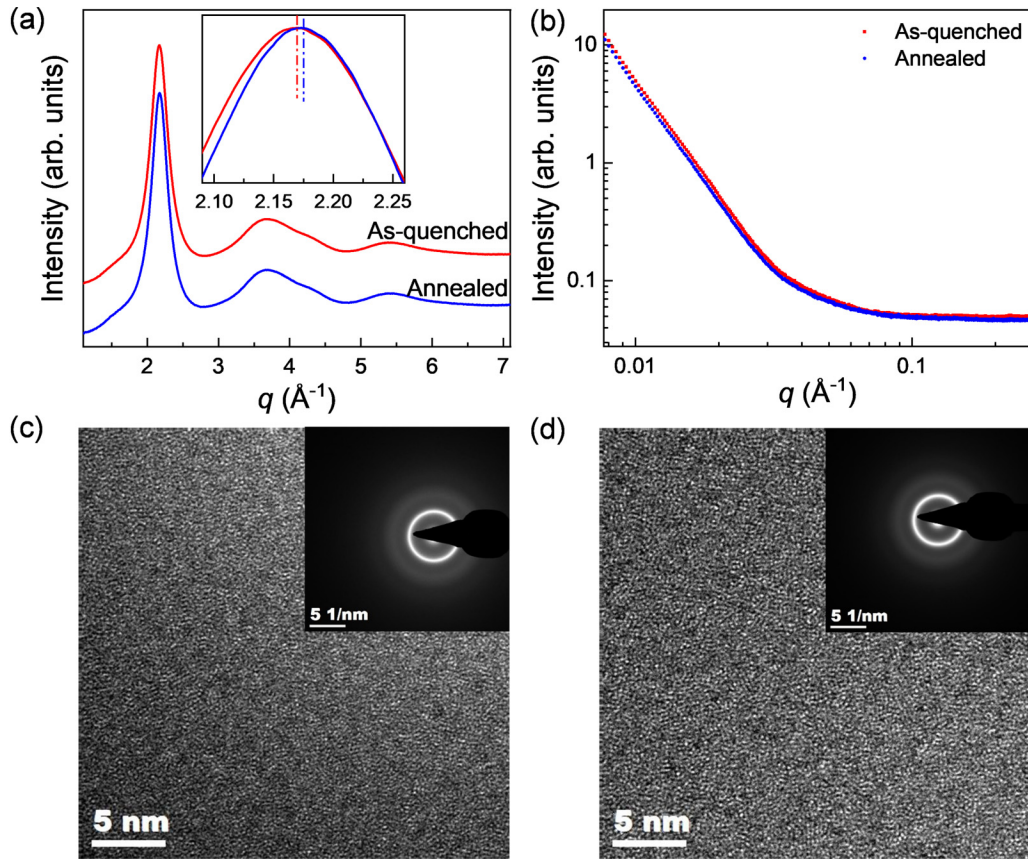


FIG. 1. Characterization of amorphous structure of the as-quenched and annealed  $\text{La}_{75}\text{Al}_{25}$  MG samples. (a) Synchrotron XRD patterns at ambient pressure. The inset depicts an enlarged view of the principal diffraction peaks. (b) Synchrotron SAXS patterns. TEM characterization of the (c) as-quenched and (d) annealed MG samples. The insets in (c) and (d) are their corresponding SAED images. The scale bars are 5 nm in the HRTEM images and  $5 \text{ nm}^{-1}$  in the SAED images.

the load on the sample displacement into surface ( $P$ - $h$ ) curves using the Oliver-Pharr method [43].

Furthermore, *in situ* high-pressure synchrotron XRD experiments were performed at beamline 15U1, SSRF. To ensure identical experimental conditions, the two samples were loaded together into the same symmetric DAC with an anvil culet of  $\sim 400 \mu\text{m}$ . Helium was used as the best pressure-transmitting medium to achieve high hydrostaticity [44,45]. A tiny piece of gold foil was loaded along the sample in the DAC as a pressure standard using the Au equation of state [46] by XRD. The pressure was controlled by a double-sided gas membrane system. The pressure in the sample chamber was carefully stabilized to make sure the pressure change before and after each exposure was less than 0.1 GPa. Background scattering signal from the high-pressure environment was collected at each pressure by shinning the x-ray beam off the sample to only penetrate the pressure medium and two diamond anvils. The x ray has a wavelength of  $0.6199 \text{ \AA}$  and a beam size of  $\sim 3 \mu\text{m} \times 2.5 \mu\text{m}$ . The exposure time was 30 s for each pressure point. The software DIOPTAS [47] was employed to integrate two-dimensional images into one-dimensional  $I(q)$  patterns ( $q = 4\pi \sin \theta / \lambda$ , where  $\lambda$  is the wavelength of the incident x ray and  $2\theta$  is the scattering angle) with the corresponding background scattering signal subtracted for each pattern.

### III. RESULTS

#### A. Characterization of the amorphous structure

Figure 1(a) shows the synchrotron XRD patterns of the as-quenched and annealed  $\text{La}_{75}\text{Al}_{25}$  MG samples at ambient pressure. The absence of sharp Bragg diffraction peaks over the entire  $q$  range indicates the fully amorphous nature of the samples. The inset of Fig. 1(a) provides a closer look at the principal peaks. The principal peak position ( $q_1$ ) of the annealed sample exhibits a shift towards a higher  $q$  value compared with the as-quenched sample, from  $2.169$  to  $2.174 \text{ \AA}^{-1}$  (increased by  $\sim 0.23\%$ ). Moreover, the peak width of the annealed sample considerably narrows, reducing from  $0.301$  to  $0.284 \text{ \AA}^{-1}$  (by  $\sim 5.65\%$ ). These results suggest that the annealing treatment results in a denser and less disordered atomic structure, namely, a state with less  $V_f$  as expected [31].

Additionally, Fig. 1(b) displays the synchrotron SAXS patterns, which decay smoothly without any discernible fluctuations. These data confirm the structural homogeneity at the nanoscale, therefore ruling out phase separation in both glass samples [48], which was further evidenced by HRTEM results [Figs. 1(c) and 1(d), respectively]. In addition, as seen in the insets of Figs. 1(c) and 1(d), the SAED images exhibit diffused halos without any observable sharp Bragg diffraction spots or rings. These results consistently suggest

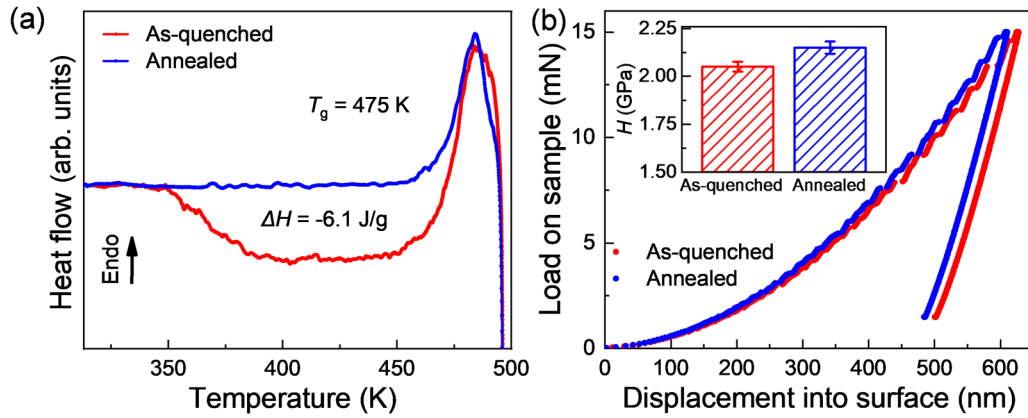


FIG. 2. Characterization of thermal and mechanical properties of the as-quenched and annealed  $\text{La}_{75}\text{Al}_{25}$  MG samples. (a) The DSC curves. (b) The  $P$ - $h$  curves from nanoindentation measurements. The determined hardness values are compared in the inset.

that, although annealing effectively reduces  $V_f$ , both the as-quenched and annealed samples possess a good amorphous microstructure, which is important for further studies on  $V_f$  variation and its effect on glass properties.

### B. Characterization of $V_f$ contents

Besides the diffraction peak shift, DSC tests are more generally employed to estimate the variation of  $V_f$  in glasses. Specifically, the exothermic signal observed prior to the glass transition in a DSC curve,  $\Delta H$ , signifies the annihilation process of  $V_f$  via structural relaxation [25,27]. Hence, the variation of  $V_f$  can be estimated by the changes of  $\Delta H$  values. As shown in Fig. 2(a), the pronounced  $\Delta H$  signal ( $-6.1$  J/g) of the as-quenched sample indicates its substantial quench in  $V_f$ . In contrast, the  $\Delta H$  signal of the annealed sample is almost eliminated, while the characteristic temperatures of  $T_g$  ( $\sim 475$  K) and  $T_x$  (crystallization temperature) remain almost unaltered. Therefore, scarce free volume is confirmed in the annealed sample while retaining a good glassy state. It should be emphasized that free volume is intrinsic for glass structures; the almost disappeared  $\Delta H$  signal in the DSC curve of the annealed sample does not mean complete annihilation of free volume. Figure 2(b) shows the  $P$ - $h$  curves of the two samples obtained from nanoindentation measurements. The maximum indentation depth in the annealed sample is smaller than that in the as-quenched sample with identical load (i.e., a higher hardness of the annealed sample), a natural consequence of an overall denser glass structure containing less  $V_f$  in the annealed state [49].

### C. Structural evolution of the two samples with different $V_f$ contents under pressure

Besides thermal annealing, pressure could also tune  $V_f$  in glasses. With an identical hydrostatic pressure environment for the as-quenched and annealed samples achieved in this work [Fig. 3(a)], their different compression behavior can be attributed to the intrinsic differences between the two samples, i.e., their different contents of  $V_f$ . Figures 3(b) and 3(c) depict the *in situ* high-pressure synchrotron XRD patterns from 2.2 to 23.1 GPa during compression and decompression of

the as-quenched and the annealed MG samples, respectively. No prominent sharp Bragg peaks are emerging in all XRD patterns, which indicates the absence of pressure-induced crystallization [40]. With increasing pressure, the principal amorphous peaks of both samples shift towards higher  $q$  values, as expected by the pressure-induced structural shrinkage.

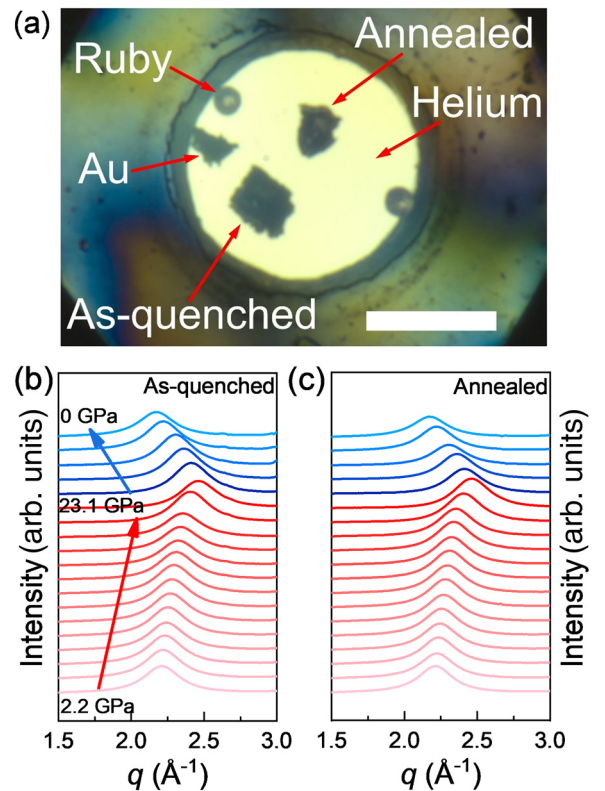


FIG. 3. *In situ* high-pressure synchrotron XRD measurement on the as-quenched and annealed  $\text{La}_{75}\text{Al}_{25}$  MG samples. (a) An image of the DAC sample chamber with two samples loaded together for an identical hydrostatic pressure environment. The scale bar represents 100  $\mu\text{m}$ . The *in situ* high-pressure synchrotron XRD patterns during compression and decompression of the as-quenched and annealed samples are shown in (b) and (c), respectively.

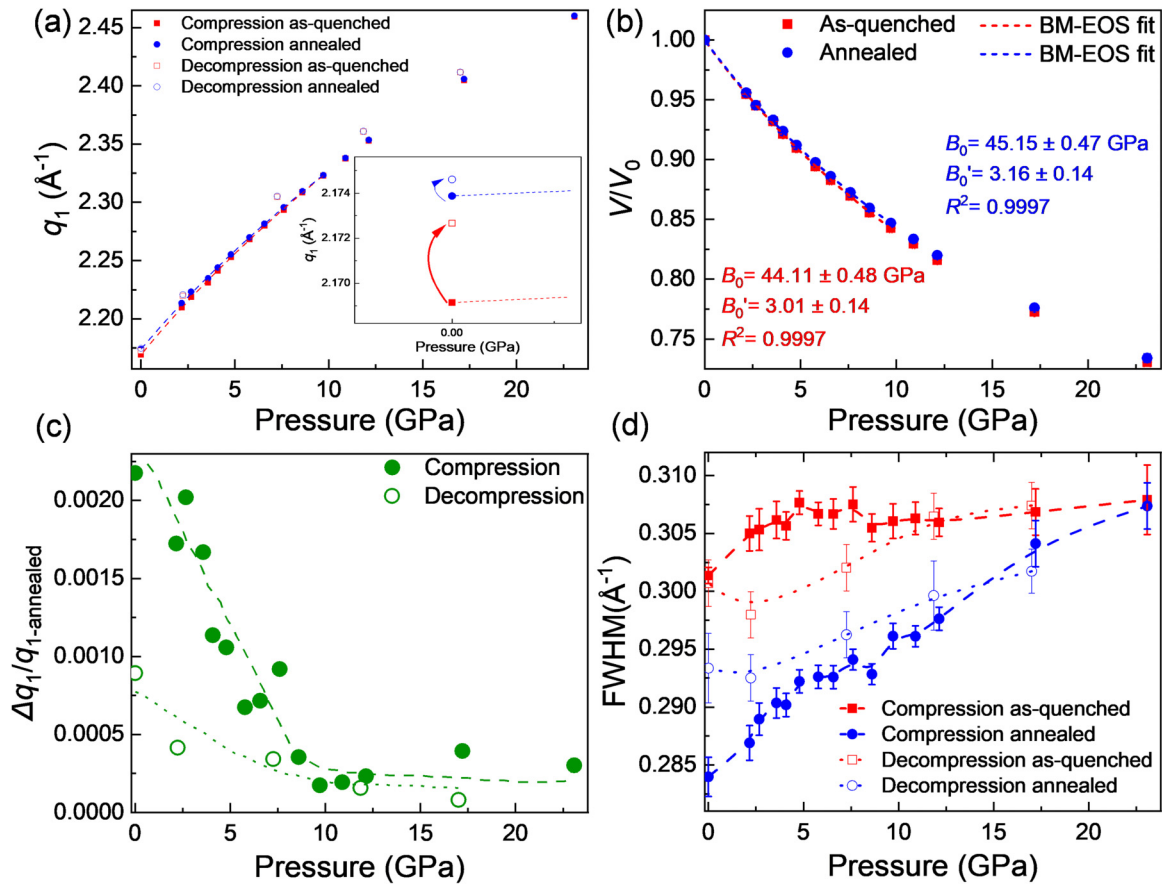


FIG. 4. Analysis of the principal diffraction peak position and width variation with pressure of the as-quenched and annealed La<sub>75</sub>Al<sub>25</sub> MG samples. (a) The  $q_1$  values of as-quenched and annealed samples as a function of pressure. The inset shows the  $q_1$  values at ambient pressure before compression (obtained separately) and after decompression. (b) The relative changes of average atomic volumes with pressure. The dotted lines in (b) and (c) are the fitting curves to the third-order BM-EOS below 10 GPa. (c) The relative changes of  $q_1$  difference between the two samples as a function of pressure calculated from  $\Delta q_1/q_{1\text{-annealed}} = (q_{1\text{-as-quenched}} - q_{1\text{-annealed}})/q_{1\text{-annealed}}$ . (d) The FWHM values of the as-quenched and annealed samples as a function of pressure. Error bars are mainly from pressure variation and fitting uncertainty, which are smaller than the symbol sizes in (a)–(c).

During decompression, the peaks return to lower  $q$  values with a seemingly elastic recovery behavior.

The synchrotron XRD patterns with a very high signal-to-noise ratio allow us to accurately determine the amorphous peak positions ( $q_1$ ) with the resolution better than  $10^{-4}$   $\text{\AA}^{-1}$  for a quantitative comparison, which is also well documented in previous studies [35]. Figure 4(a) shows the  $q_1$  values obtained by fitting the principal amorphous peaks in XRD patterns as a function of pressure using a Voigt profile and a linear baseline (more details of the fitting can be found in the Supplemental Material, Fig. S1 [50]). During compression, slight differences (e.g.,  $\Delta q_1 = 0.004$   $\text{\AA}^{-1}$  at 2.2 GPa) in  $q_1$  of the two samples can be observed at low pressures; specifically, the annealed sample shows slightly larger  $q_1$  values than the as-quenched sample, which is consistent with the characterization at ambient condition shown in Fig. 1(a). However, the differences in  $q_1$  between the two samples decrease quickly with increasing pressure and almost disappear (e.g.,  $\Delta q_1 = 0.0007$   $\text{\AA}^{-1}$  at 23.1 GPa) above  $\sim 10$  GPa. Upon decompression,  $q_1$  does not reversibly retrace the compression curves but consistently remains larger than the values during compression, exhibiting a hysteresis for both samples.

Moreover, a closer look at the data in the inset of Fig. 4(a) shows that the as-quenched sample initially with a higher content of  $V_f$  (smaller  $q_1$ ) presents obvious permanent densification after complete pressure release, while the annealed sample almost recovers its initial state. Specifically, the relative differences between the recovered  $q_1$  and the initial  $q_1$  are 0.16% and 0.03% for the as-quenched and annealed samples, respectively.

It is well established that  $q_1$  can be used to estimate the change of average atomic volume in MGs using a simple power-law relation,  $V_a \propto (1/q_1)^D$  [51]. The power exponent  $D$  was determined to be  $\sim 2.5$  for La-based MGs under high pressure [36,37]. Therefore, here we use the equation  $V(P)/V(0) = [q_1(0)/q_1(P)]^{2.5}$  to estimate the relative atomic volume change under pressure,  $V/V_0$ , as shown in Fig. 4(b). The relative atomic volume change of the as-quenched sample under pressure is slightly larger than that of the annealed sample, which confirms that the as-quenched sample with higher content of  $V_f$  is indeed more compressible. By fitting the pressure-dependent  $V/V_0$  data (below 10 GPa) to the third-order Birch-Murnaghan isothermal equation of state (BM-EOS) [52], the isothermal bulk modulus ( $B_0$ ) and

the pressure derivative ( $B'_0$ ) can be obtained. For the as-quenched sample,  $B_0 = 44.11 \pm 0.48$  GPa and  $B'_0 = 3.01 \pm 0.14$ , while for the annealed sample,  $B_0 = 45.15 \pm 0.47$  GPa and  $B'_0 = 3.16 \pm 0.14$ , close to the previously reported bulk moduli of La-based MGs obtained by the ultrasonic sound velocity technique [53]. Considering their identical compositions but different bulk moduli corresponding to different  $V_f$  contents, most likely, regions rich in free volume also sustain a considerable portion of stress, participating in the compression process. The extra free volume in the as-quenched sample accounts for the smaller bulk modulus and could be squeezed out by pressure. Therefore, the as-quenched sample gradually approaches the annealed state in terms of closer  $q_1$  values (less free volume), as shown in Fig. 4(a). Quantitatively, the rate at which the extra free volume in the as-quenched sample was compressed can be estimated by the change of the relative difference in  $q_1$ , i.e.,  $(q_{1-\text{as-quenched}} - q_{1-\text{annealed}})/q_{1-\text{annealed}}$ , as shown in Fig. 4(c). At the beginning, as pressure increases, the relative difference in  $q_1$  decreases linearly and quickly approaches zero at  $\sim 10$  GPa and remains around zero beyond 10 GPa. Upon pressure release, the relative difference in  $q_1$  partially recovers but is still much lower than the initial values, again suggesting permanent changes in their density difference ( $V_f$  contents). Interestingly, the recovery of the relative difference in  $q_1$  also follows a linear relationship, suggesting a general and robust trend for the changes of  $V_f$  in MGs.

Besides the principal diffraction peak position  $q_1$ , the peak width also carries rich information on glass structures. Generally, a broader peak means a more disordered or heterogeneous glass structure [54,55]. As shown in Fig. 4(d), the fitted full width at half maximum (FWHM) values of the principal diffraction peak were determined during compression and decompression for both samples. The initial FWHM of the annealed sample is smaller than that of the as-quenched sample, consistent with our expectation of a denser and more ordered glass state after annealing. For the as-quenched sample, during compression, its FWHM increases at the beginning and then quickly stabilizes at  $\sim 5$  GPa. During decompression, the FWHM mirrors the compression trend at higher pressures before swiftly declining between 10 and 5 GPa. Ultimately, the FWHM nearly reverts to its initial (prior to compression) value.

In contrast, for the annealed sample, the FWHM variation is quite different from that of the as-quenched sample. The FWHM increases sharply and continuously up to 23.1 GPa with a slight decrease of the increase rate at  $\sim 5$  GPa. At 23.1 GPa, the FWHM of the annealed sample overlaps with that of the as-quenched sample. During decompression, the FWHM also shows a hysteresis below  $\sim 10$  GPa above the compression trajectory. When pressure is released, the FWHM exhibits noticeable, permanent broadening in the annealed sample. Both samples seem to behave quite differently, and the variation of FWHM is much more complex than that of the peak position, providing extra information on the glass structure in MGs.

#### IV. DISCUSSION

It is well accepted that an amorphous structure usually has a lower overall packing density than its crystalline counter-

part. Pressure-induced structural permanent densification is not a rare phenomenon in a wide range of glassy systems. The pressure-induced permanent densification of  $\text{SiO}_2$  glass can be as high as  $\sim 21\%$  after high-pressure treatment at room temperature. This is attributed to the highly compressible open network amorphous structure of  $\text{SiO}_2$  glass, which enables coordinate number increases by intertetrahedral angle variation [32]. In the case of MGs, their densely packed structure with already very high nearest-neighbor coordination numbers (up to 12–14) at ambient conditions usually rules out the possibility of having typical pressure-induced densification by changing coordination numbers. Some previous studies on MGs reported slight permanent densification after high-pressure treatment at high temperatures [56–59], which was attributed to possible local rearrangement of atomic structures via thermally activated diffusion. Instead, during compression at room temperature, the free volume can be compressed elastically, but no permanent annihilation or reduction was observed, suggesting a pretty homogeneous distribution of free volume in a stiff matrix [31].

In principle, there are no equivalent atoms and/or molecules in glasses due to the lack of strict symmetry [28]. Therefore, even under hydrostatic pressure, although the overall compression or deformation is homogeneous, the local elastic deformation could be slightly inhomogeneous and nonaffine. Above a certain threshold, irreversible structural rearrangement could occur even at temperatures far below  $T_g$ . This scenario could rationalize what we observed in Fig. 4(c). Below  $\sim 10$  GPa, the linear behavior of  $V_f$  reduction is similar to the case of the  $\text{Cu}_{46}\text{Zr}_{46}\text{Al}_8$  MG [31], in which the non-affine deformation might still be recoverable. Once pressure is high enough (with respect to the bulk modulus of the sample), the  $V_f$  reduction (deformation) may resemble “plastic-like deformation” of  $V_f$  with a constant content above 10 GPa. At this stage, the compression or annihilation of  $V_f$  is locally so severe, becoming partially irreversible upon decompression. These results reveal the existence of a critical pressure required to trigger the permanent pressure-induced densification in MGs, which was not achieved in the previous reports on the  $\text{Cu}_{46}\text{Zr}_{46}\text{Al}_8$  MG up to 30 GPa, probably due to its relatively high bulk modulus [31]. According to the extensively proposed simplified heterogeneous structural model of MGs with soft liquidlike (containing relatively more  $V_f$ ) domains embedded in a hard solidlike matrix (containing relatively less  $V_f$ ) [18,19], at the beginning of compression, stress will be mainly sustained by the rigid matrix of the solidlike regions. Therefore, we will expect a critical pressure to reach a highly compressible stage; i.e., when the stress increases beyond the instability limit of the solidlike matrix, the soft liquidlike regions or domains start to engage in the deformation with enhanced compressibility [the data in Fig. 4(c) should show a larger slope at high pressures], which, however, contradicts the linear compression followed by a saturation behavior of  $V_f$  as seen in the current work. Therefore, a structural model with more homogeneously mixed  $V_o$  and  $V_f$  over a large length scale seems more reasonable [31].

Regarding the diffraction peak width, the decreased FWHM value after annealing is in line with our typical expectation that annealing annihilates free volume (reducing the soft liquidlike regions) and therefore homogenizes the glass

structure [60]. However, under high pressure, although we also expect free-volume annihilation, the FWHM values of both samples do not decrease as in the annealing case but increase consistently, which indicates that besides densification considerable local stress and/or strain is also built up during compression. Intriguingly, the pressure dependency of the FWHM of the annealed sample is much more pronounced than that of the as-quenched sample. Based on the scenario of the local elastic heterogeneous model, the as-quenched sample with a relatively high content of  $V_f$  could more easily cease the local stress and/or strain accumulation due to a relatively low “yielding pressure” to trigger the plastic deformation of  $V_f$ , e.g., showing a steady state (saturation) of FWHM above 5 GPa. In contrast, the annealed sample relatively lacks easily deformable  $V_f$  (soft liquidlike regions); therefore, local stress and/or strain continuously builds up during compression up to 23.1 GPa, leading to persistent diffraction peak broadening. Under substantial local stress during compression, additional irreversible nonaffine structural rearrangements might occur, potentially leading to the entrenchment of permanent peak broadening. These results could bring new structural insights into the unusual compression-induced rejuvenation and relaxation dynamics anomaly at room temperature observed in Ce-based MGs [33,61,62].

## V. SUMMARY

In summary, our study employed *in situ* high-pressure synchrotron XRD to explore the compression and decompression behaviors of the two  $\text{La}_{75}\text{Al}_{25}$  binary MGs with distinct free-volume contents. Our experimental approach allowed a precise determination of differences in diffraction peak position and peak width between the two samples under high pressure, offering detailed insights into the glass structure based on the free-volume framework. A linear compression behavior of the free volume followed by a saturation stage above 10 GPa is confirmed in the  $\text{La}_{75}\text{Al}_{25}$  MGs.

Thermal annealing below the glass transition temperature reduces free volume and structural heterogeneity in terms of density fluctuation. In contrast, while pressure typically leads to a reduction of free volume elastically, compressing beyond a critical pressure could also induce permanent reduction of free volume. Even hydrostatic pressure also causes a buildup of local stress and/or strain in both MG samples due to intrinsic local heterogeneity in mechanical properties. The MG with a higher free-volume content displays more significant permanent densification but surprisingly less pronounced pressure sensitivity in local stress and/or strain buildup. These results could help to validate prevailing structural models based on the free-volume concept and inspire more realistic models that capture the intricate complexities of glass structure, particularly regarding spatial heterogeneity and its thermal and mechanical responses.

## ACKNOWLEDGMENTS

The authors acknowledge financial support from Shanghai Key Laboratory of Material Frontiers Research in Extreme Environments, China (Grant No. 22dz2260800) and the Shanghai Science and Technology Committee, China (Grant No. 22JC1410300), and the National Natural Science Foundation of China (Grant No. 52101187). The XRD experiments were performed at beamline 15U1 of the Shanghai Synchrotron Radiation Facility (SSRF). The SAXS experiments were performed at beamline 12-IDB, Advanced Photon Source (APS), Argonne National Laboratory (ANL). The APS is a U.S. Department of Energy (DOE) Office of Science User Facility operated for the DOE Office of Science by ANL under Contract No. DE-AC02-06CH11357. The authors thank H. Shu from HPSTAR for his kind help with the gas loading system and Dr. X. Zou for his help with the SAXS measurement. Part of this work also used beamline 16B1, SSRF, China.

- 
- [1] T. G. Fox, Jr., and P. J. Flory, Second-order transition temperatures and related properties of polystyrene. I. Influence of molecular weight, *J. Appl. Phys.* **21**, 581 (1950).
  - [2] H. Eyring, Viscosity, plasticity, and diffusion as examples of absolute reaction rates, *J. Chem. Phys.* **4**, 283 (1936).
  - [3] E. B. Bagley and J. M. Scigliano, Free volume of liquids and polymers from internal pressure studies, *Polym. Eng. Sci.* **11**, 177 (1971).
  - [4] J. C. Dyre, Colloquium: The glass transition and elastic models of glass-forming liquids, *Rev. Mod. Phys.* **78**, 953 (2006).
  - [5] M. H. Cohen and D. Turnbull, Molecular transport in liquids and glasses, *J. Chem. Phys.* **31**, 1164 (1959).
  - [6] K. Rätzke, P. W. Hüppe, and F. Faupel, Transition from single-jump type to highly cooperative diffusion during structural relaxation of a metallic glass, *Phys. Rev. Lett.* **68**, 2347 (1992).
  - [7] A. K. Doolittle, Studies in Newtonian flow. II. The dependence of the viscosity of liquids on free-space, *J. Appl. Phys.* **22**, 1471 (1951).
  - [8] M. H. Cohen and G. S. Grest, Liquid-glass transition, a free-volume approach, *Phys. Rev. B* **20**, 1077 (1979).
  - [9] D. Turnbull and M. H. Cohen, Free-volume model of the amorphous phase: Glass transition, *J. Chem. Phys.* **34**, 120 (1961).
  - [10] P. Wen, M. B. Tang, M. X. Pan, D. Q. Zhao, Z. Zhang, and W. H. Wang, Calorimetric glass transition in bulk metallic glass forming Zr-Ti-Cu-Ni-Be alloys as a free-volume-related kinetic phenomenon, *Phys. Rev. B* **67**, 212201 (2003).
  - [11] A. van den Beukel and J. Sietsma, The glass transition as a free volume related kinetic phenomenon, *Acta Metall. Mater.* **38**, 383 (1990).
  - [12] O. Haruyama and A. Inoue, Free volume kinetics during sub- $T_g$  structural relaxation of a bulk  $\text{Pd}_{40}\text{Ni}_{40}\text{P}_{20}$  metallic glass, *Appl. Phys. Lett.* **88**, 131906 (2006).
  - [13] A. R. Yavari, A. L. Moulec, A. Inoue, N. Nishiyama, N. Lupu, E. Matsubara, W. J. Botta, G. Vaughan, M. D. Michiel, and Å. Kvick, Excess free volume in metallic glasses measured by x-ray diffraction, *Acta Mater.* **53**, 1611 (2005).

- [14] Z. Evenson and R. Busch, Equilibrium viscosity, enthalpy recovery and free volume relaxation in a  $Zr_{44}Ti_{11}Ni_{10}Cu_{10}Be_{25}$  bulk metallic glass, *Acta Mater.* **59**, 4404 (2011).
- [15] M. Zhang, Y. M. Wang, F. X. Li, S. Q. Jiang, M. Z. Li, and L. Liu, Mechanical relaxation-to-rejuvenation transition in a Zr-based bulk metallic glass, *Sci. Rep.* **7**, 625 (2017).
- [16] P. S. Steif, F. Spaepen, and J. W. Hutchinson, Strain localization in amorphous metals, *Acta Metall.* **30**, 447 (1982).
- [17] A. S. Argon and H. Y. Kuo, Plastic flow in a disordered bubble raft (an analog of a metallic glass), *Mater. Sci. Eng.* **39**, 101 (1979).
- [18] W. Dmowski, T. Iwashita, C. P. Chuang, J. Almer, and T. Egami, Elastic heterogeneity in metallic glasses, *Phys. Rev. Lett.* **105**, 205502 (2010).
- [19] J. C. Ye, J. Lu, C. T. Liu, Q. Wang, and Y. Yang, Atomistic free-volume zones and inelastic deformation of metallic glasses, *Nat. Mater.* **9**, 619 (2010).
- [20] Y. Shi and M. L. Falk, Stress-induced structural transformation and shear banding during simulated nanoindentation of a metallic glass, *Acta Mater.* **55**, 4317 (2007).
- [21] X. J. Liu, G. L. Chen, X. Hui, T. Liu, and Z. P. Lu, Ordered clusters and free volume in a Zr–Ni metallic glass, *Appl. Phys. Lett.* **93**, 011911 (2008).
- [22] T. G. Fox and P. J. Flory, The glass temperature and related properties of polystyrene. Influence of molecular weight, *J. Polym. Sci.* **14**, 315 (1954).
- [23] K. M. Flores, D. Suh, R. H. Dauskardt, P. Asoka-Kumar, P. A. Sterne, and R. H. Howell, Characterization of free volume in a bulk metallic glass using positron annihilation spectroscopy, *J. Mater. Res.* **17**, 1153 (2011).
- [24] R. T. Ott, M. J. Kramer, M. F. Besser, and D. J. Sordelet, High-energy x-ray measurements of structural anisotropy and excess free volume in a homogeneously deformed Zr-based metallic glass, *Acta Mater.* **54**, 2463 (2006).
- [25] Z. Evenson and R. Busch, Enthalpy recovery and free volume relaxation in a  $Zr_{44}Ti_{11}Ni_{10}Cu_{10}Be_{25}$  bulk metallic glass, *J. Alloys Compd.* **509**, S38 (2011).
- [26] R. P. White and J. E. G. Lipson, Polymer free volume and its connection to the glass transition, *Macromolecules* **49**, 3987 (2016).
- [27] A. Slipenyuk and J. Eckert, Correlation between enthalpy change and free volume reduction during structural relaxation of  $Zr_{55}Cu_{30}Al_{10}Ni_5$  metallic glass, *Scr. Mater.* **50**, 39 (2004).
- [28] S. V. Ketov, Y. H. Sun, S. Nachum, Z. Lu, A. Checchi, A. R. Beraldin, H. Y. Bai, W. H. Wang, D. V. Louzguine-Luzgin, M. A. Carpenter *et al.*, Rejuvenation of metallic glasses by non-affine thermal strain, *Nature (London)* **524**, 200 (2015).
- [29] A. J. Matheson, Role of free volume in the pressure dependence of the viscosity of liquids, *J. Chem. Phys.* **44**, 695 (1966).
- [30] W. H. Wang, The elastic properties, elastic models and elastic perspectives of metallic glasses, *Prog. Mater. Sci.* **57**, 487 (2012).
- [31] S. Chen, D. Xu, X. Zhang, X. Chen, Y. Liu, T. Liang, Z. Yin, S. Jiang, K. Yang, J. Zeng *et al.*, Reversible linear-compression behavior of free volume in a metallic glass, *Phys. Rev. B* **105**, 144201 (2022).
- [32] T. Rouxel, H. Ji, T. Hammouda, and A. Moréac, Poisson's ratio and the densification of glass under high pressure, *Phys. Rev. Lett.* **100**, 225501 (2008).
- [33] T. P. Ge, C. Wang, J. Tan, T. Ma, X. H. Yu, C. Q. Jin, W. H. Wang, and H. Y. Bai, Unusual energy state evolution in Ce-based metallic glass under high pressure, *J. Appl. Phys.* **121**, 205109 (2017).
- [34] H. Rösner, M. Peterlechner, C. Kübel, V. Schmidt, and G. Wilde, Density changes in shear bands of a metallic glass determined by correlative analytical transmission electron microscopy, *Ultramicroscopy* **142**, 1 (2014).
- [35] H. F. Poulsen, J. A. Wert, J. Neuefeind, V. Honkimäki, and M. Daymond, Measuring strain distributions in amorphous materials, *Nat. Mater.* **4**, 33 (2005).
- [36] Q. Zeng, Y. Kono, Y. Lin, Z. Zeng, J. Wang, S. V. Sinogeikin, C. Park, Y. Meng, W. Yang, H. K. Mao *et al.*, Universal fractional noncubic power law for density of metallic glasses, *Phys. Rev. Lett.* **112**, 185502 (2014).
- [37] Q. Zeng, Y. Lin, Y. Liu, Z. Zeng, C. Y. Shi, B. Zhang, H. Lou, S. V. Sinogeikin, Y. Kono, C. Kenney-Benson *et al.*, General 2.5 power law of metallic glasses, *Proc. Natl. Acad. Sci. USA* **113**, 1714 (2016).
- [38] H. W. Sheng, E. Ma, H. Z. Liu, and J. Wen, Pressure tunes atomic packing in metallic glass, *Appl. Phys. Lett.* **88**, 171906 (2006).
- [39] G. Li, Y. Y. Wang, P. K. Liaw, Y. C. Li, and R. P. Liu, Electronic structure inheritance and pressure-induced polyamorphism in lanthanide-based metallic glasses, *Phys. Rev. Lett.* **109**, 125501 (2012).
- [40] Q. Zeng, H. Sheng, Y. Ding, L. Wang, W. Yang, J. Z. Jiang, W. L. Mao, and H. K. Mao, Long-range topological order in metallic glass, *Science* **332**, 1404 (2011).
- [41] Q. S. Zeng, Y. Ding, W. L. Mao, W. Yang, S. V. Sinogeikin, J. Shu, H. K. Mao, and J. Z. Jiang, Origin of pressure-induced polyamorphism in  $Ce_{75}Al_{25}$  metallic glass, *Phys. Rev. Lett.* **104**, 105702 (2010).
- [42] Q. Luo, G. Garbarino, B. Sun, D. Fan, Y. Zhang, Z. Wang, Y. Sun, J. Jiao, X. Li, P. Li *et al.*, Hierarchical densification and negative thermal expansion in Ce-based metallic glass under high pressure, *Nat. Commun.* **6**, 5703 (2015).
- [43] W. C. Oliver and G. M. Pharr, An improved technique for determining hardness and elastic modulus using load and displacement sensing indentation experiments, *J. Mater. Res.* **7**, 1564 (2011).
- [44] X. Chen, H. Lou, Z. Zeng, B. Cheng, X. Zhang, Y. Liu, D. Xu, K. Yang, and Q. Zeng, Structural transitions of 4:1 methanol-ethanol mixture and silicone oil under high pressure, *Matter Radiat. Extremes* **6**, 038402 (2021).
- [45] P. Loubeyre, R. LeToullec, D. Hausermann, M. Hanfland, R. J. Hemley, H. K. Mao, and L. W. Finger, X-ray diffraction and equation of state of hydrogen at megabar pressures, *Nature (London)* **383**, 702 (1996).
- [46] O. L. Anderson, D. G. Isaak, and S. Yamamoto, Anharmonicity and the equation of state for gold, *J. Appl. Phys.* **65**, 1534 (1989).
- [47] C. Prescher and V. B. Prakapenka, DIOPTAS: A program for reduction of two-dimensional x-ray diffraction data and data exploration, *High Press. Res.* **35**, 223 (2015).
- [48] A. A. Kündig, M. Ohnuma, T. Ohkubo, and K. Hono, Early crystallization stages in a Zr–Cu–Ni–Al–Ti metallic glass, *Acta Mater.* **53**, 2091 (2005).



- [49] N. Li, L. Liu, Q. Chen, J. Pan, and K. C. Chan, The effect of free volume on the deformation behaviour of a Zr-based metallic glass under nanoindentation, *J. Phys. D* **40**, 6055 (2007).
- [50] See Supplemental Material at <http://link.aps.org/supplemental/10.1103/PhysRevB.109.214201> for a representative XRD peak profile fitting.
- [51] D. Ma, A. D. Stoica, and X. L. Wang, Power-law scaling and fractal nature of medium-range order in metallic glasses, *Nat. Mater.* **8**, 30 (2009).
- [52] T. Katsura and Y. Tange, A simple derivation of the Birch-Murnaghan equations of state (EOSs) and comparison with EOSs derived from other definitions of finite strain, *Minerals* **9**, 745 (2019).
- [53] Q. K. Jiang, G. Q. Zhang, L. Yang, X. D. Wang, K. Saksli, H. Franz, R. Wunderlich, H. Fecht, and J. Z. Jiang, La-based bulk metallic glasses with critical diameter up to 30 mm, *Acta Mater.* **55**, 4409 (2007).
- [54] A. P. Sokolov, A. Kisliuk, M. Soltwisch, and D. Quitmann, Medium-range order in glasses: Comparison of Raman and diffraction measurements, *Phys. Rev. Lett.* **69**, 1540 (1992).
- [55] H. Lou, Z. Zeng, F. Zhang, S. Chen, P. Luo, X. Chen, Y. Ren, V. B. Prakapenka, C. Prescher, X. Zuo *et al.*, Two-way tuning of structural order in metallic glasses, *Nat. Commun.* **11**, 314 (2020).
- [56] R. J. Xue, L. Z. Zhao, C. L. Shi, T. Ma, X. K. Xi, M. Gao, P. W. Zhu, P. Wen, X. H. Yu, C. Q. Jin *et al.*, Enhanced kinetic stability of a bulk metallic glass by high pressure, *Appl. Phys. Lett.* **109**, 221904 (2016).
- [57] R. Yamada, Y. Shibazaki, Y. Abe, W. Ryu, and J. Saida, Unveiling a new type of ultradense anomalous metallic glass with improved strength and ductility through a high-pressure heat treatment, *NPG Asia Mater.* **11**, 72 (2019).
- [58] W. Dmowski, G. H. Yoo, S. Gierlotka, H. Wang, Y. Yokoyama, E. S. Park, S. Stelmakh, and T. Egami, High pressure quenched glasses: Unique structures and properties, *Sci. Rep.* **10**, 9497 (2020).
- [59] H. J. Jin, X. J. Gu, P. Wen, L. B. Wang, and K. Lu, Pressure effect on the structural relaxation and glass transition in metallic glasses, *Acta Mater.* **51**, 6219 (2003).
- [60] F. Zhu, H. K. Nguyen, S. X. Song, D. P. B. Aji, A. Hirata, H. Wang, K. Nakajima, and M. W. Chen, Intrinsic correlation between  $\beta$ -relaxation and spatial heterogeneity in a metallic glass, *Nat. Commun.* **7**, 11516 (2016).
- [61] X. Zhang, H. Lou, B. Ruta, Y. Chushkin, F. Zontone, S. Li, D. Xu, T. Liang, Z. Zeng, H.-k. Mao *et al.*, Pressure-induced nonmonotonic cross-over of steady relaxation dynamics in a metallic glass, *Proc. Natl. Acad. Sci. USA* **120**, e2302281120 (2023).
- [62] Q. Zeng, In situ high-pressure wide-angle hard x-ray photon correlation spectroscopy: A versatile tool probing atomic dynamics of extreme condition matter, *Matter Radiat. Extremes* **8**, 028101 (2023).